International Journal of Environmental Science and Technology (2023) 20:11471–11482
https://doi.org/10.1007/s13762-023-05122-1

ORIGINAL PAPER

High-performance aggregate production by sintering terra rossa containing pyrophyllite and colloidal calcite

M. U. Toprak[1] · C. Karakurt[2] · Y. Kibici[3] · V. Uz[4] · F. Sen[5] · F. Bilen[1]

Received: 6 April 2023 / Revised: 31 May 2023 / Accepted: 13 July 2023 / Published online: 28 July 2023
© The Author(s) under exclusive licence to Iranian Society of Environmentalists (IRSEN) and Science and Research Branch, Islamic Azad University 2023

Abstract

The demand for high-performance lightweight concrete in the construction industry has increased the need for higher-strength and lightweight aggregates compared to existing aggregates. Terra rossa (TR) containing pyrophyllite and colloidal-sized calcite was evaluated as a raw material in the production of aggregate. Small cylinders (15 × 15 mm) were prepared with (TR) to investigate the effect of water content, molding force, drying time, and different sintering temperatures on the physical, mechanical, mineralogical properties and microstructure of aggregates. According to SEM observations, increasing the molding force considerably decreased the porosity and the amount of partially bonded grains. The highest aggregate strength (145 MPa) was obtained for 15% water content, 27 kN molding force, and sintering at 900 °C in aggregate production. The particle density was 2.04 g/cm^3, while it was 2.22 and 2.38 for 1000 and 1100 °C. Colloidal size calcite helped to reduce the particle density by forming pores thanks to gas generation. The glassy phase formed in the body more than necessary decreased the strength (82 MPa) due to the brittle structure at 1000 °C. The mullite phase developed at 1100 °C with the aid of pyrophyllite enhanced the aggregate strength up to 117 MPa. The performance of sintered TR aggregate in concrete can be investigated within the scope of future studies.

Keywords Aggregates · Concrete · Microstructure · Mineralogy · Sintering · Terra rossa

Introduction

Concrete is the most widely used building material in the construction industry. Reducing the concrete unit weight reduces the earthquake forces acting on the structure while providing superior heat and sound insulation characteristics to concrete (Real et al. 2016; Kalpana and Tayu 2020; Siamardi 2022). Aggregates account for 75% or more of the concrete volume (Kim et al. 2021). Thus, intensive studies have been carried out on the production of lightweight aggregates. Concrete has a density of 2240–2480 kg/m^3 made with ordinary aggregates (sand, gravel, crushed stone) and is defined as normal weight concrete (NWC), while structural lightweight concrete (SLC) has a minimum 28-day compressive strength of 17 MPa, an equilibrium density between 1120 and 1920 kg/m^3, and consists entirely of lightweight aggregate or a combination of lightweight and normal density aggregate (Akers et al. 2003). Aggregates, which were utilized in NWC, are generally local dolomite or limestone, with a specific gravity of 2650–2800 kg/m^3. Lightweight expanded clay aggregates (LECAs) are preferably used to produce SLC. Particle density and crushing resistance of common and structural LECA acquired from an Iranian LECA factory were given for different size ranges in Table 1 (Ardakani and Yazdani 2014).

The porous nature of LECA considerably decreases the mechanical properties of concrete. Therefore, this weakness

Editorial responsibility: Agnieszka Galuszka.

M. U. Toprak and F. Sen have contributed equally to this work.

✉ M. U. Toprak
mugur.toprak@dpu.edu.tr

[1] Department of Civil Engineering, Kütahya Dumlupınar University, 43100 Kutahya, Türkiye

[2] Department of Civil Engineering, Bilecik Seyh Edebali University, 11100 Bilecik, Türkiye

[3] Department of Construction Technology, Bilecik Seyh Edebali University, 11100 Bilecik, Türkiye

[4] Department of Materials Engineering, Kütahya Dumlupınar University, 43100 Kutahya, Türkiye

[5] Sen Research Group, Department of Biochemistry, Kütahya Dumlupınar University, 43000 Kutahya, Türkiye

Table 1 Properties of common and structural LECA (Ardakani and Yazdani 2014)

LECA type	Group name	Size range (mm)	Mean size (mm)	Particle dry density (kg/m^3)	Crushing resistance (MPa)
Common	C1	3.36–4.76	4.1	695	1.74
	C2	6.35–8.0	7.2	580	1.17
	C3	8.0–11.2	9.6	503	0.87
	C4	12.7–16.0	14.3	481	0.82
Structural	S1	3.36–4.76	4.1	1106	3.62
	S2	6.35–8.0	7.2	871	3.01
	S3	8.0–11.2	9.6	828	2.11
	S4	12.7–16.0	14.3	806	2.15

should be improved to enhance the mechanical properties of SLC (Rutherford 1987; Dabbaghi et al. 2021). In addition, LECA is manufactured from special raw plastic clay and it is not locally available (Rutherford 1987; Chiadighikaobi and Tarka 2021). Therefore, researching abundant sources suitable for high strength and lightweight aggregate production is inevitable. TR is found along with fractures and between bedding surfaces in karstic regions of both mediterranean and aegean regions of Turkey (Atalay 1997). But literature about their sintering behaviors is rather limited (Cengiz and Kuşçu 2010).

TR belongs to the red lateritic soils of the mediterranean climate regions of the zonal soils group. TR typically occurs as a discontinuous layer that ranges from a few centimeters to several meters in thickness that covers limestone and dolomite bedrock. For the formation of these soils, the presence of the mediterranean climate type and the calcareous main material is an absolute condition (Durn et al. 1999; Torrent 2005; Vingiani et al. 2018). They are a complex mixture of silicates (clays, micas, quartz), carbonates (dolomite, calcite), and oxide/oxyhydroxide minerals (hematite, goethite), with a variety of different functional groups. The most dominant mineral phases in the clay fraction of the TR soils are kaolinites and illites, followed by vermiculite and smectite materials. The most important characteristics of TR are their free Fe_2O_3 (hematite) content usually between 4 and 6%, which gives bright red colors. Soil formed on the grayish-blue crystalline limestones of TR has been found to have very little residual material. The most important chemical process here is decalcification, and the water-soluble $CaCO_3$ is removed by washing (Sattari et al. 2013; Stipičević et al. 2014). After decalcification, very little calcite may remain with the clay. Since chemical analysis is not sufficient to determine this, a detailed mineralogical analysis should be done either under a polarizing microscope by making thin sections or a detailed X-ray analysis.

The liquid-phase production during heat treatment is made feasible by the mineral makeup of TR soils. The burned bodies' deformation and shrinkage are controlled by quartz. As a flux, alkaline-rich feldspar creates a quasi-liquid phase that has an impact on the densification process and ultimate porosity (Das and Dana 2003; Diella et al. 2015). The most characteristic types of red soil over carbonate rocks are TR. The novelty of this study is the utilization of terra rossa soils in lightweight and strong artificial aggregate production as an alternative material against expanded clay aggregates. Sintering behaviors of TR were investigated in order to obtain high-performance structural aggregate for LWC production.

Materials and methods

The main raw material of this study is TR that was obtained from Çöğürler-Kütahya/Turkey. This area is occupied by mountain terrains/highlands, which are built up of different rock types but dominated by (marbles) meta-carbonate rocks as presented in Fig. 1.

The density of the TR was determined as 2.51 g/cm^3 according to TS EN 1097-6. TR was ground by a ringed mill for 3 min to increase the surface area from 2738 to 4847 cm^2/gr. TR cylinders (TRCs) were produced by mixing TR with water, molding inside the 15-mm cylinder mold (Fig. 2a), drying at 20 ± 2 °C for 1 day, and sintering. The content of the water used in shaping aggregate (WC) 5, 10, 15, and 20% by weight of TR. Three different molding forces (MF) were applied on TR specimens at 1, 3, 15, and 27 kN to obtain proper compaction and shaping. The drying time (DT) of TR is 1, 2, and 3 days; then, it was subjected to exposure of sintering temperatures (ST) at 900, 1000, and 1100 °C. The sintering process was performed in a laboratory furnace with a heating rate of 10 °C/min and by an

Fig. 1 Terra rossa formation on the limestone layer in Çöğürler (Kütahya/Turkey) complex

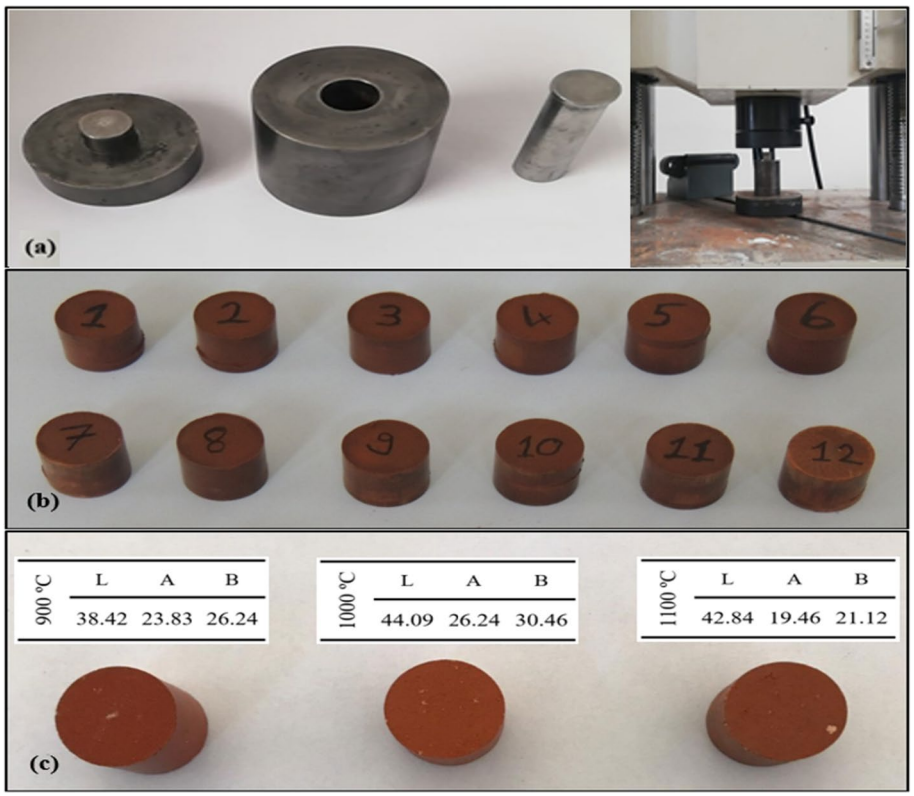

Fig. 2 **a** Cylinder mold and molding by press **b** raw TRC, and **c** sintered TRC

exposure time of 5 min at max temperature and then allowed to cool in it to 20 °C. In the first stage, 12 series consisting of 48 TRC were produced by mixing TR with water, drying at 20 ± 2 °C for 1 day, and molded under molding force of 3 kN inside the 15 mm cylinder mold (Fig. 2a). The particle density (PD) of TR was determined in accordance with TS EN 1097-6. The TRC specimens were labeled according to WC-MF-DT-ST, respectively (e.g. TRC-10-3-2-1100).

Firstly, the effect of WC and DT was evaluated on 12 series consisting of 48 TRC, while MF and ST were

constant (3 kN and 1100 °C). Then, extra 12 cylinders were prepared to obtain the effect of molding force (1–3 to 15–27 kN) on the series having the highest specific strength. Finally, the effects of sintering temperatures (900, 1000, and 1100 °C) were evaluated. The molded raw TRC and sintered TRC at 900, 1000, and 1100 °C are presented in Fig. 2b and c. TG–DTA analysis is performed at 50–1150 °C with a heating and cooling rate of 10 and

20 °C/min in a dry air atmosphere with a flow rate of 40 ml/min. The mechanical strength of the final product was achieved by performing uniaxial compressive strength (UCS) test at a 0.6 MPa/s loading rate. The mineralogical properties of the raw TR and hardened TRC were carried out by using X-ray diffraction (XRD) manufactured by Panalytical. XRD of the raw TR was investigated on the floating colloid portion of the suspension, which was prepared as a mixture of TR and water and left to rest for one day. The microstructure of the broken parts of TRC was determined by using a Zeiss SUPRA 40VP scanning electron microscope (SEM).

Results and discussion

Chemical and mineralogical properties of TR

The XRF analysis of the TR is presented in Table 2. The TR was mainly composed of SiO_2, Al_2O_3, and Fe_2O_3 containing a low amount of alkaline oxides. The presence of K_2O may be associated with the presence of illite and also potassic feldspars (Azevedo et al. 2018). Major soil-forming processes in the area are leaching of calcium carbonate and accumulation in the dominant form of hematite mineral.

The most important characteristics of TR are Fe_2O_3. nH_2O (limonite) and Fe_2O_3 (hematite) minerals content, which gives yellow/orange, bright red colors, and up to 10%, usually between 4 and 6%. It shows similarity to lateritic soils due to their red color and iron content. The LOI of TR about 15.26% by wt. was relatively high. By contrast, the percentage of fluxing components (alkaline and alkaline earth oxides) was low. The high percentage of LOI shows an elevated fraction of clay minerals; the meaningful amount of Fe_2O_3 in both raw materials gives specimens the reddish color after firing as illustrated by Vigneron et al. (2019).

Table 2 Chemical composition of terra rossa

Oxide content	SiO_2	Al_2O_3	Na_2O	K_2O	Fe_2O_3	CaO	MgO	MnO	TiO_2	Cl	SO_3	*LOI
% mass	56.07	15.98	0.14	1.93	6.52	1.91	1.27	0.11	0.57	0.06	0.05	15.25

*Loss on ignition

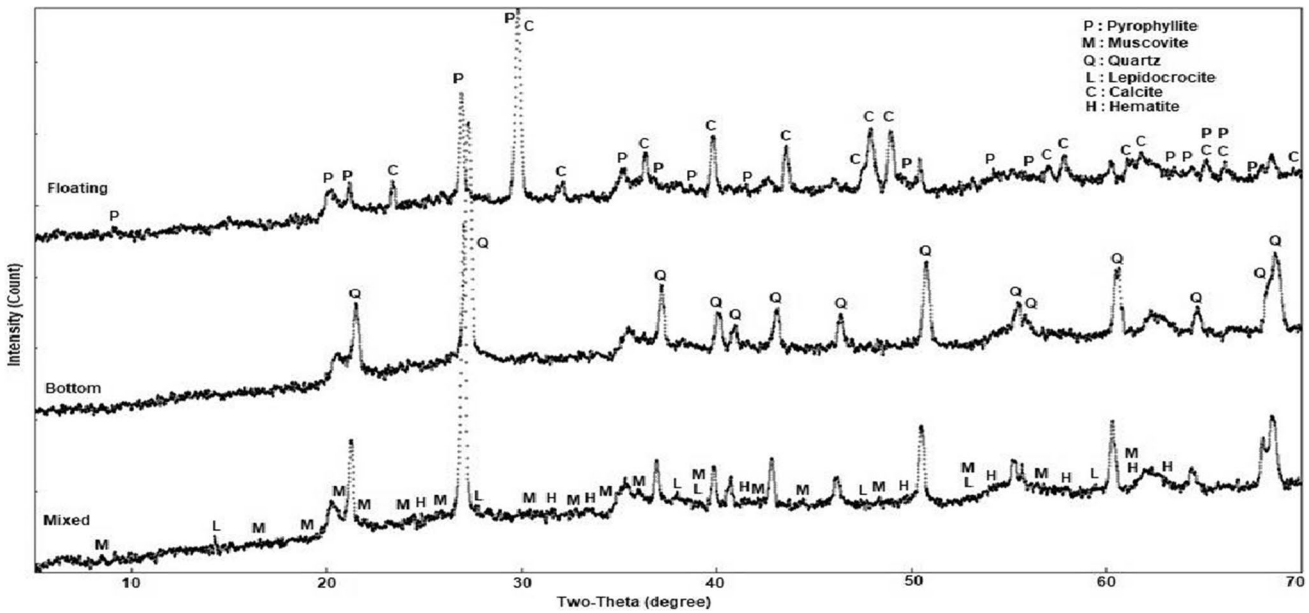

Fig. 3 XRD analysis of terra rossa [floating, precipitated (bottom) and mixed parts]

When XRD analysis (Fig. 3) is performed on the TR without separating the fine-grained part by sedimentation, many peaks of muscovite, calcite, and pyrophyllite were not evident. It has been observed that the fine-grained part consists of the peaks of pyrophyllite, calcite, and lepidocrocite minerals. In the precipitated part, besides quartz minerals, some peaks of pyrophyllite and hematite were also determined. Although the pyrophyllite is more prominent in the floating part, the precipitation being in the coarse part indicates that the fine-grained pyrophyllite crystals are more visible. As calcite is not observed in the coarse part but is evident in the fine part, it is thought to be colloid particles. The colloid particles of calcite may be effective in creating nano-sized pores during the sintering phase.

Thermal analysis of terra rossa

Kaolinitic clays cause an increase in their strength with the development of mullite crystals during the sintering stage. Similar to kaolinitic clays, pyrophyllite increases the strength of TR by the development of acicular mullite crystals during sintering. The proportions of the glassy phase and mullite crystals affect the strength of sintered TR aggregates. In Fig. 4, the thermogravimetric (TGA) curves of TR were reported. Weight losses of 8% have been observed up to 1100 °C. The differential thermal analysis (DTA) traces of the TR show two big endothermic peaks between 40–160 °C and 370–540 °C, corresponding to evaporation of free water (2.5%) and crystalline water (4%), respectively. Poorly crystalline kaoline probably be detected in the general noise of XRD spectra, while sharp peaks of kaolin were not detected.

In the low-temperature domain of the calcination reaction (500–800 °C), the transformation of kaolinite into metakaolin is characterized by the removal of the chemically bonded water and the breakdown of the hydroxyl bonds (Drits and Derkowski 2015; Guatame-García et al. 2018). The weight losses up to 900 °C can be associated with the dehydration of clay minerals. The amorphous silica liberated during the metakaolin decomposition is highly reactive, possibly assisting eutectic melt formation at 990 °C (Sonuparlak et al. 1987; Carty and Senapati 1998). The sample develops a glassy phase at temperatures above 900 °C. As the temperature continues to increase, porosity is eliminated via viscous-phase sintering. The densification phenomenon always led to shrinkage of the ceramic body during heating (i.e., firing shrinkage) (Roy et al. 2010; Ergul et al. 2011).

The sintering temperatures of the aggregates were determined as 3 stages according to the thermal analysis. The first of these temperatures, 900 °C, was chosen as the point with an endothermic peak onset and a distinctive peak in the DTA curve. At the same time, it was chosen because fine-grained calcite in clay calcite decomposes after 850 °C to provide a gaseous release and to create porosity in the body. 1000 °C, which is the peak of the exothermic peak, and

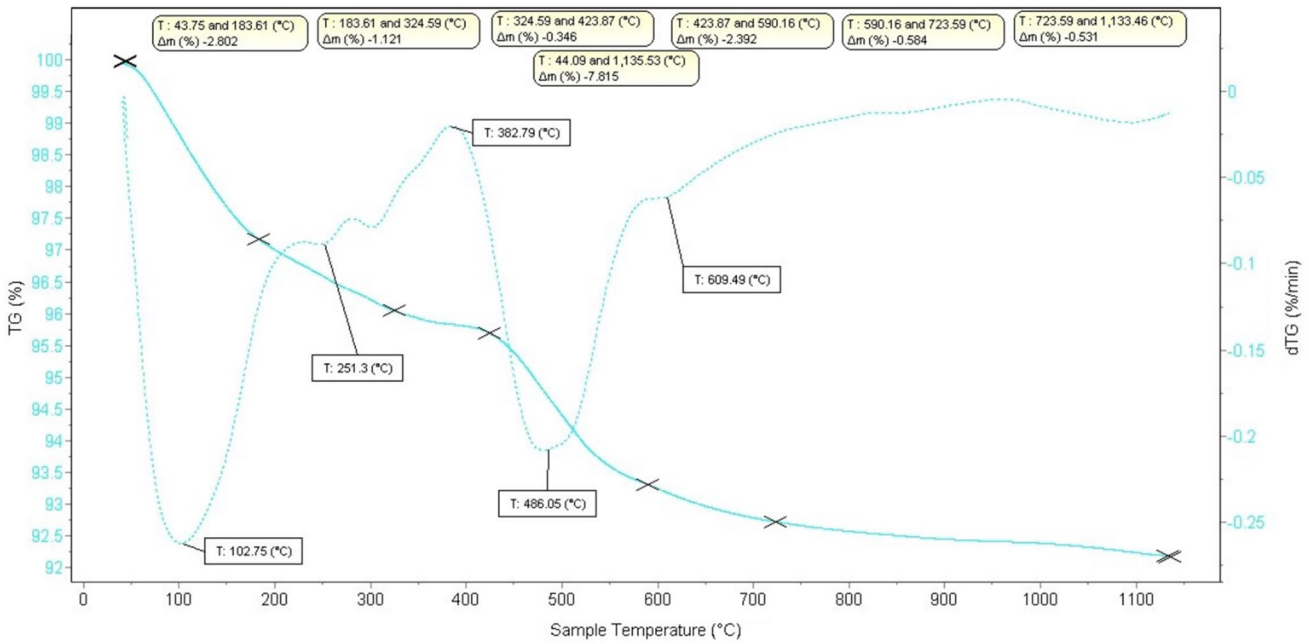

Fig. 4 Thermal analysis of the terra rossa

1100 °C, which is the middle of the region where it enters the endothermic trend, were also chosen.

Physical and mechanical test results

The plasticity of the clays varies according to the clay mineral it contains and the ratios of the other minerals found next to it. For this reason, it is important to determine the amount of water to be used in the shaping phase of the clay used according to the ceramic product to be produced. Insufficient water use in shaping reduces the grain–grain interaction in clays, resulting in insufficient packaging and insufficient strength to develop. On the other hand, excessive use of water causes the distance between the grains to widen and the clay layers to slide easily over each other, resulting in weak dried and sintered strengths. For this reason, determining the amount of water required for each clay product is effective in the final product properties. The volume (V), mass (M), particle density (PD) of the raw specimen (RS), 1, 2, or 3 days air-dried and sintered TRC and UCS of TRC are given in Table 3.

PD of dried TRC increases with increasing WC but tends to decrease after 15% WC. Likewise, the PD and the compressive strengths of the sintered TRC increase up to 15% water content and decrease after this point. Excessive volume reduction could decrease the compressive strength of aggregate due to deformation of the body. PD enhanced 18.34, 13.29, 11.11, and 9.04% after sintering for TRC having DT of 2 days and WC of 5, 10 15, and 20%, respectively. On the other hand, UCS for mentioned TRC was 15.86, 16.52, 37.01, and 33.96 MPa, respectively.

Thus, densification ratios of TRC were not directly proportional to the UCS of the specimens. This was interpreted as insufficient packaging and insufficient strength of dried TRC produced with insufficient WC. It has been determined that a 15% WC and 2 days of DT is the most appropriate ratio during the shaping process in aggregate production. Effect of molding force on TRC prepared with constant 15%

Table 3 Physical and mechanical properties of TRC according to DT and WC%

Specimen code	Dried TRC												Sintered TRC	
	V (cm^3)				M (g)				PD (g/cm^3)				PD (g/cm^3)	UCS (MPa)
	DT (day)													
	RS	1	2	3	RS	1	2	3	RS	1	2	3		
TRC-5-3-1-1100	2.95	2.93			4.95	4.90			1.68	1.68			1.89	15.98
TRC-5-3-2-1100	2.80	2.79	2.78		4.80	4.70	4.70		1.71	1.69	1.69		2.00	15.86
TRC-5-3-3-1100	2.82	2.80	2.79	2.79	4.79	4.73	4.68	4.68	1.70	1.69	1.68	1.68	1.89	20.61
TRC-10-3-1-1100	2.94	2.89			5.00	4.93			1.73	1.71			1.87	15.75
TRC-10-3-2-1100	2.83	2.75	2.75		4.98	4.75	4.75		1.76	1.73	1.73		1.96	16.52
TRC-10-3-3-1100	2.84	2.78	2.77	2.75	5.00	4.87	4.83	4.80	1.76	1.75	1.74	1.74	1.99	21.19
TRC-15-3-1-1100	2.71	2.66			5.45	5.00			2.02	1.88			2.04	35.12
TRC-15-3-2-1100	2.62	2.60	2.58		5.13	4.70	4.65		1.96	1.81	1.80		2.00	37.01
TRC-15-3-3-1100	2.66	2.64	2.61	2.60	5.28	4.89	4.80	4.77	1.98	1.85	1.84	1.83	2.06	43.90
TRC-20-3-1-1100	2.61	2.56			4.95	4.60			1.90	1.80			1.91	29.78
TRC-20-3-2-1100	2.59	2.53	2.50		4.95	4.57	4.42		1.91	1.81	1.77		1.93	33.96
TRC-20-3-3-1100	2.59	2.49	2.46	2.45	4.96	4.55	4.38	4.34	1.92	1.83	1.78	1.77	1.97	38.83

Table 4 Physical and mechanical properties of dried and sintered TRC according to MF

Specimen code	Dried TRC			Sintered TRC			
	V (cm^3)	M (g)	PD (g/cm^3)	V (cm^3)	M (g)	PD (g/cm^3)	UCS (MPa)
TRC-15-1-2-1100	2.71	4.42	1.63	2.13	3.97	1.86	15.21
TRC-15-3-2-1100	2.58	4.65	1.80	2.12	4.25	2.00	37.01
TRC-15-15-2-1100	2.33	4.69	2.01	1.98	4.48	2.26	74.67
TRC-15-27-2-1100	2.16	4.45	2.06	1.75	4.16	2.38	117.82

Table 5 Physical and mechanical properties of dried and sintered TRC according to ST

Specimen code	Dried			Sintered			
	V (cm^3)	M (g)	PD (g/cm^3)	V (cm^3)	M (g)	PD (g/cm^3)	UCS (MPa)
TRC-15-27-2-900	2.14	4.38	2.07	2.05	4.00	2.04	144.68
TRC-15-27-2-1000	2.17	4.51	2.08	1.88	4.10	2.22	82.97
TRC-15-27-2-1100	2.16	4.45	2.06	1.75	4.03	2.38	117.82

WC and 2 days DT is evaluated in Table 4. When pressed up to 1, 3, 15, and 27 kN, PD of the sintered TRC was 1.86, 2.00, 2.20, and 2.38 g/cm^3, respectively. Corresponding UCS of them was 15.21, 37.01, 74.67, and 117.82 MPa, respectively. In the shaping of clay products, the force to be applied in shaping is effective in the properties of the final product. The bulk densities increase with increasing forming force because the grains are closer to each other and the intergranular spaces are reduced and the packaging is better. Therefore, the strength increases with the increase of intergranular reaction in sintering.

Finally, the effects of sintering temperatures (900, 1000, and 1100 °C) are evaluated in Table 5. Excessive glassy phase development in the presence of minerals such as feldspar as a melting reduces the strength. For this reason, it is necessary to determine the sintering temperature by knowing the other minerals besides the clays. The PD of the TRC sintered at 900 °C is 2.04 g/cm^3, with the lowest value. This shows that calcite decomposes and forms porosity in the aggregate. At the same time, the highest value in compressive strengths (144.68 MPa) was obtained at 900 °C.

Porosity decreases and density increases at higher sintering temperatures with microstructural changes due to enhancement of glassy phase. The glassy phase infiltrated the pores of the structure and caused densification as illustrated in literature (Milheiro et al. 2005; Özkan and Yayla 2016). However, the compressive strength of the TRC decreased with the increase of the glassy phase. According to the physical and mechanical properties, the appropriate firing temperature was determined to be 900 °C. Sintered terra rossa aggregate reached compressive strengths of 144.68 MPa, and it was approximately 25% lighter than limestone aggregate. By using carbonates (Na_2CO_3 and $CaCO_3$) as expansion agents as illustrated by Martínez et al. 2018, lighter aggregates can be produced by sintering TR.

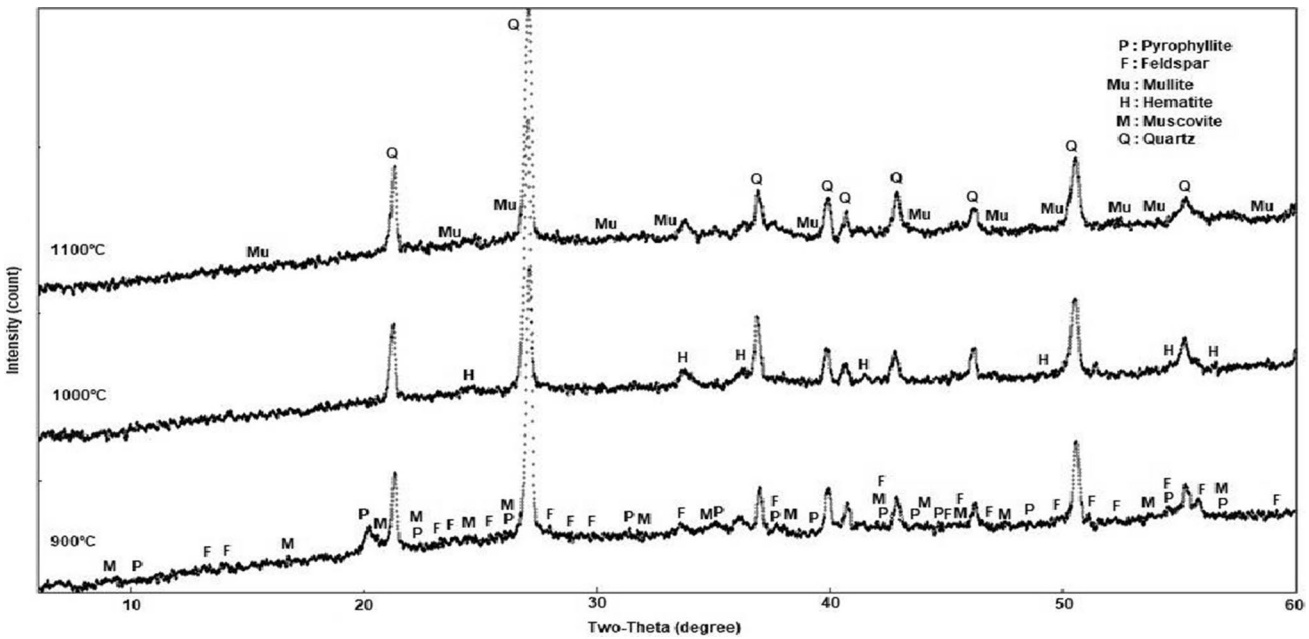

Fig. 5 The XRD patterns of sintered terra rossa cylinders

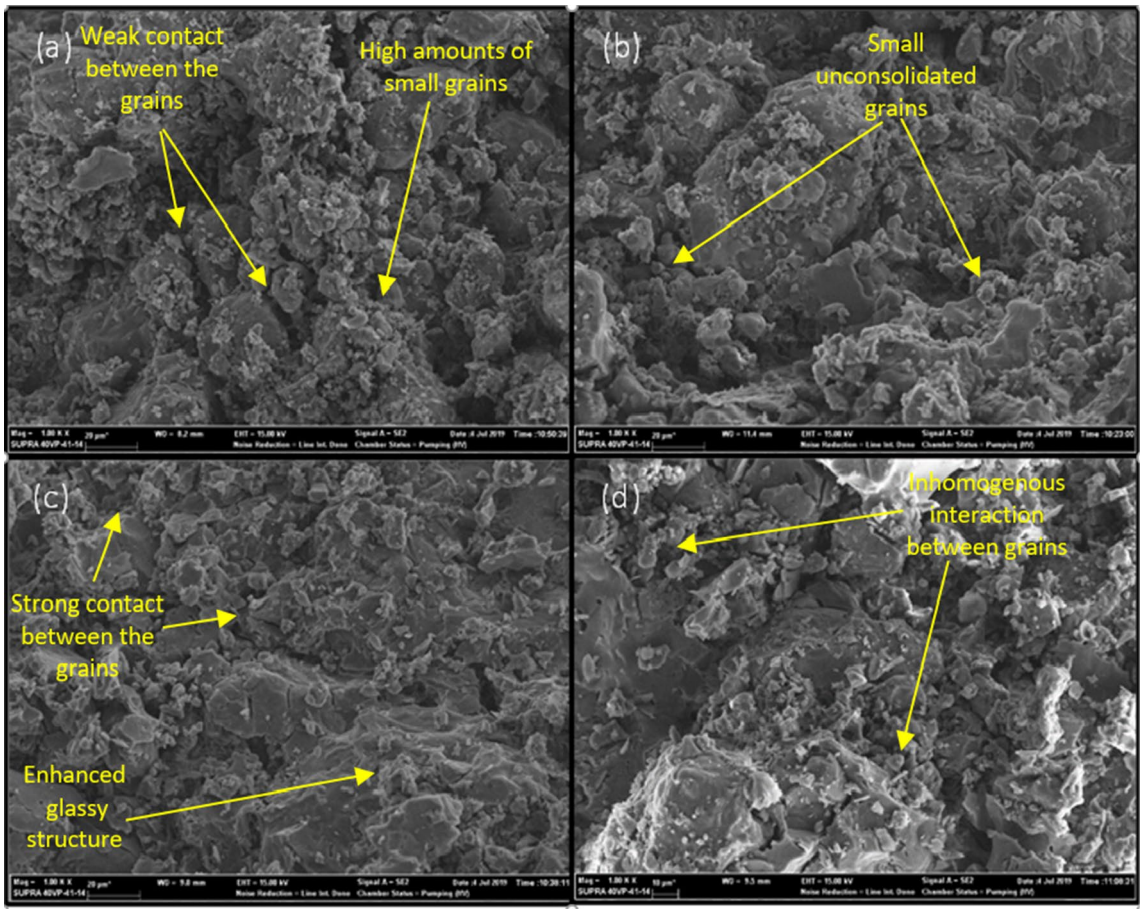

Fig. 6 SEM (1000×) of sintered TRC for different WC **a** 5%, **b** 10%, **c** 15%, and **d** 20%

XRD analysis of sintered TR aggregates

Hard limestone and dolomite-based mountain soils formed in the Mediterranean region are typically leached of their carbonate minerals and have hues ranging from brown to red. The major clay in the TR soils in Israel has been thought to be either kaolinite or montmorillonite. Studies on the development and stability of additional clay minerals in red Mediterranean soils are extremely rare (Torrent and Cabedo 1986; Sandler et al. 2015). Calcite is not usually found in well-developed TR soils, at least in the upper horizons. The coarse-sized fractions of TR soils are composed primarily of quartz, with minor quantities of feldspar, calcite, and heavy minerals (Uz 2010). The hematite phase showed its strongest peak at 900 °C (Fig. 5).

It was determined that the pyrophyllite phase was still present in the aggregates that were kept at 900 °C, but there was no peak in the aggregates sintered at 1000 °C. It was determined that the main phase was quartz in the fired aggregates and there were traces of mullite, muscovite, feldspar, and hematite. Especially in aggregates fired at 1100 °C, it was determined that the mullite phase begins to develop significantly to the left of the quartz peak at 26 two theta degrees. In addition, the presence of muscovite contributes to the formation of glassy phase by decomposing at 1000 °C (Uz 2010).

Microstructural investigation

SEM evaluations of sintered TRC produced with constant MP (3 kN) and DT (2 days) for different WC, made based on the apparent differences between the pore structure and bonding of the grains at Fig. 6. The bulk density decreases as it becomes difficult for the grains to converge when insufficient water is used in shaping clay products. It has been determined that the microstructure of the aggregates shaped at different water contents has an increasing density of grains up to 15% WC. It is also found that the contact of the grains

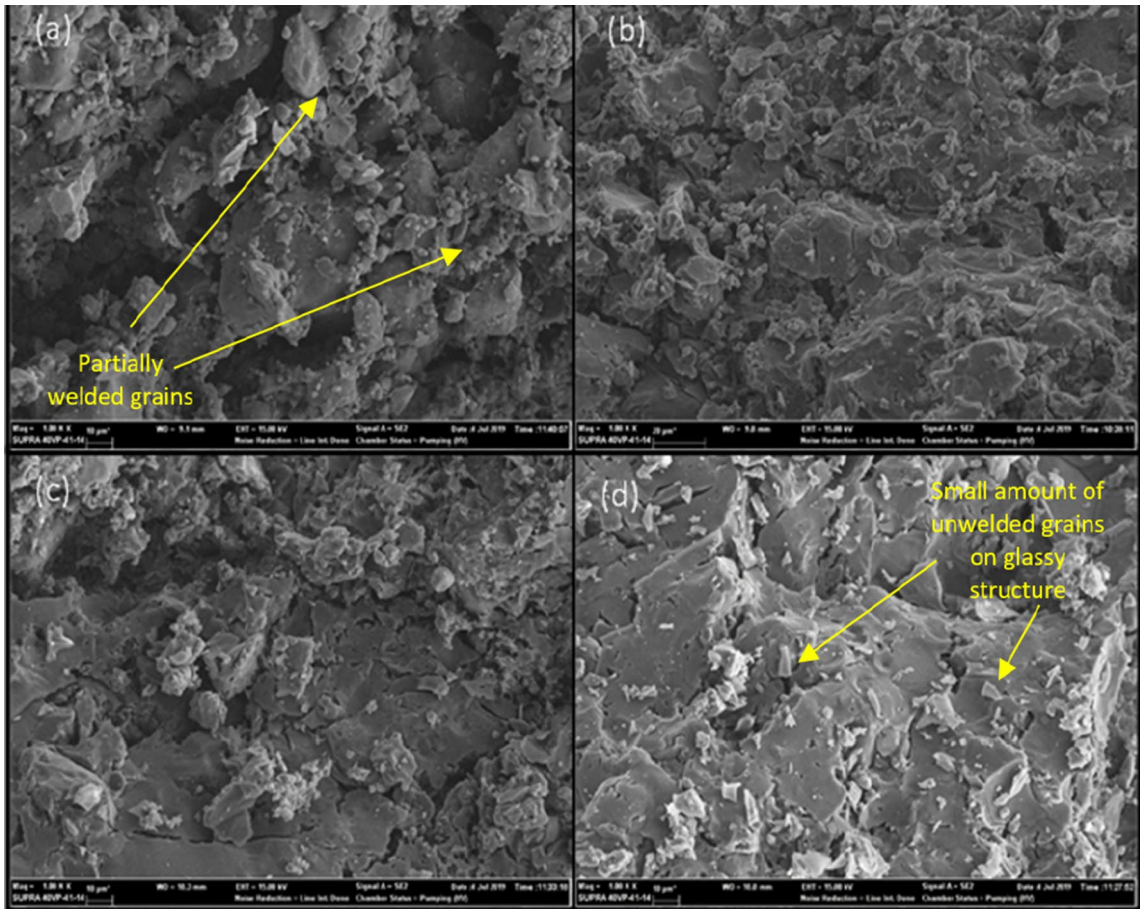

Fig. 7 SEM (1000×) of sintered TRC for MF of **a** 1 kN, **b** 3 kN, **c** 15 kN, and **d** 27 kN

shaped at the minimum water content is poor and the glassy phase is less due to the inability of the particles to react with each other during sintering.

It has been observed that the glassy structure enhanced at 15% WC. Interaction between grains in 20% WC is not homogeneous. It has been determined that the most suitable water content is 15% in aggregates produced with different water contents, and the crystals and grains formed after baking is in a much more regular and specific orientation. According to these, it can be concluded that when clay products are shaped with optimum water content, the grains are easily oriented and have a positive effect on physical properties.

Specimens having low WC (5 and 10%) have more and smaller unconsolidated grains compared to specimens having 15% and 20% WC. In the sample having 15% WC (Fig. 6c), the vitreous structure was enhanced, intergranular voids almost closed, and grain-to-grain contacts considerably increased. Thus, the compressive strength enhanced up to 37 MPa. It was concluded that the increasing WC enhanced the compactness of the raw sample. This was probably responsible for the strength behavior. Afterward, for constant WC (15%) and DT (2 days) the effect of different molding forces (3, 9, 15, and 27 kN) is evaluated in Fig. 7. The vitrification enhanced with the increase in MF. Partially welded grains were reduced under a pressing force of 15 kN (Fig. 7c). An increase in bulk density and strength is expected as the grains get closer to each other with increasing pressure. With the increasing compression pressure, denser structures can be formed as the grains come closer to each other and the packaging increases. In addition, due to the increased pressure, the samples had higher density, and grain-to-grain interaction increased, resulting in better intergranular reactions and the enhancement of the glassy phase. It was determined that in the aggregates shaped at the lowest pressure, too many finer particles were found and the particles could not interact with each other. At the highest forming pressure, however,

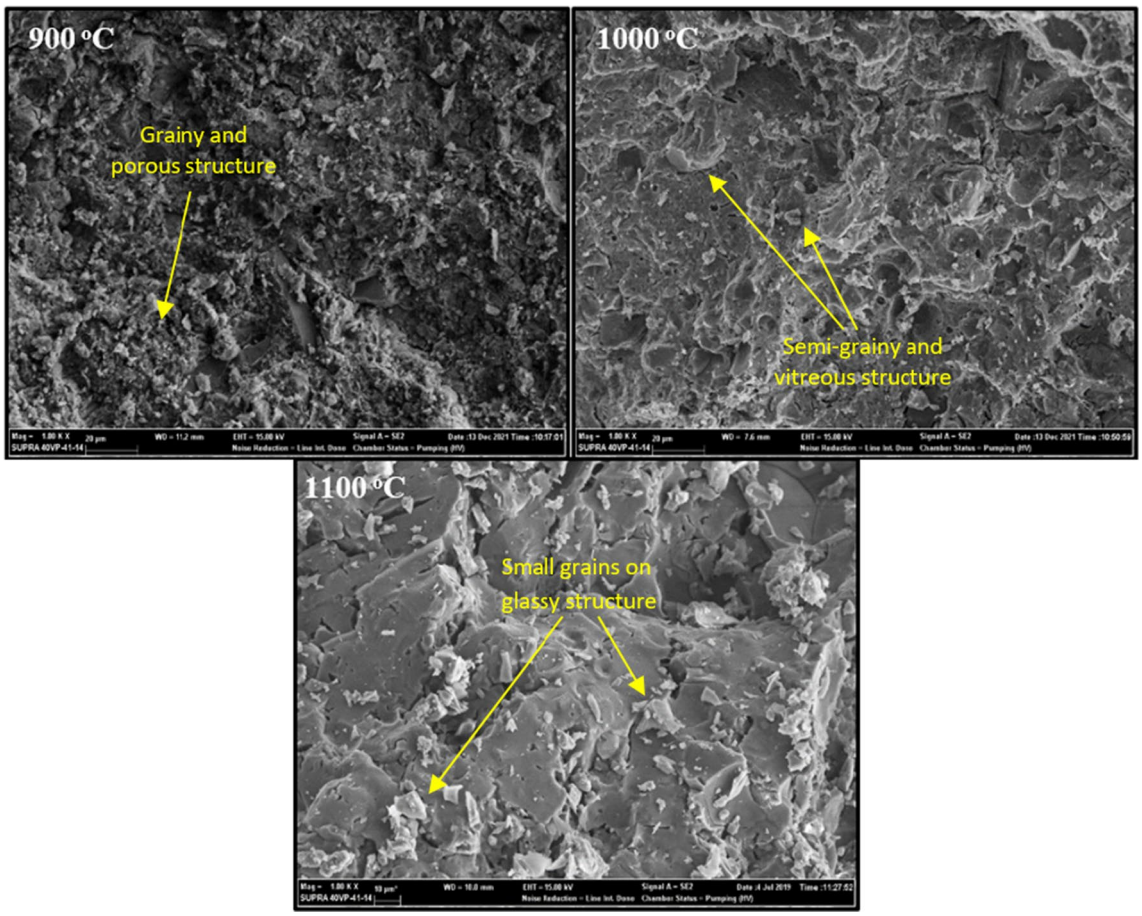

Fig. 8 SEM (1000×) of TRC sintered at 900, 1000, and 1100 °C

the number of free fines was very low and the body developed in a dense glassy phase with fewer voids.

Almost all the grains were vitrified and very few crystals were observed on the vitreous structure (Fig. 7d). Thus, the compressive strength enhanced up to 117 MPa indicating a higher packing for 27 kN. Depending on the increasing sintering temperature, the particle density and strength of the bodies increase according to the glassy phase ratio formed in the body. However, if the glassy phase is formed in the body more than necessary, the strengths will tend to decrease due to brittle structure. The microstructures of the aggregates fired at different temperatures at the lowest (900 °C) and the highest temperatures (1100 °C) are given in Fig. 8. It has been determined that the body has a porous structure at low temperatures, and a denser structure is formed with the increase of the glassy phase with increasing temperature.

Conclusion

It has been determined that colloidal calcite and pyrophyllite containing terra rossa can be used as an alternative to expanded clays in the production of lightweight aggregates. The colloid particles of calcite may be effective in creating nano-sized pores during the sintering phase. The particle density of the aggregate was considerably lower (2.04 g/cm^3) when compared with the limestone aggregate (2.7–2.85 g/cm^3). SEM images revealed that the aggregates shaped at the appropriate water content and molding force had a denser structure and the grains were oriented due to the high grain-to-grain interaction after sintering. Considering the particle density and strength, it was determined that the most suitable water content was 15%, the forming pressure was 27 kN, and the sintering temperature was 900 °C in the production of aggregates using colloidal

calcite and pyrophyllite containing TR. Increased temperatures resulted in higher density and lower strength aggregate due to excessive formation of glassy phase. The formation of mullite phases at 1100 °C enhanced the aggregate strength compared to strength at 1000 °C. Using expansion agents can be researched for producing lighter aggregates.

Acknowledgements The authors wish to thank all who assisted in conducting this work.

Declarations

Conflict of interest All authors have no conflicts of interest

References

Akers DJ, Gruber RD, Ramme BW et al (2003) Guide for structural lightweight-aggregate concrete. ACI 213R-03 Am Concr Inst (ACI), Michigan

Ardakani A, Yazdani M (2014) The relation between particle density and static elastic moduli of lightweight expanded clay aggregates. Appl Clay Sci 93–94:28–34. https://doi.org/10.1016/j.clay.2014.02.017

Atalay I (1997) Red Mediterranean soils in some karstic regions of taurus mountains, Turkey. CATENA 28:247–260. https://doi.org/10.1016/S0341-8162(96)00041-0

Azevedo ARG, França BR, Alexandre J et al (2018) Influence of sintering temperature of a ceramic substrate in mortar adhesion for civil construction. J Build Eng 19:342–348. https://doi.org/10.1016/j.jobe.2018.05.026

Carty WM, Senapati U (1998) Porcelain? Raw materials, processing, phase evolution, and mechanical behavior. J Am Ceram Soc 81:3–20. https://doi.org/10.1111/j.1151-2916.1998.tb02290.x

Cengiz O, Kuşçu M (2010) Anamasdağları-Isparta terra rossalarının tuğla-kiremit üretiminde kullanılabilirliği. Kil Bilim Teknol 1:287–299

Chiadighikaobi PC, Tarka RO (2021) Economic evaluation of expanded clay basalt fiber concrete in Nigeria structural construction. Mater Today Proc 44:4924–4930. https://doi.org/10.1016/j.matpr.2020.11.950

Dabbaghi F, Dehestani M, Yousefpour H et al (2021) Residual compressive stress–strain relationship of lightweight aggregate concrete after exposure to elevated temperatures. Constr Build Mater 298:123890. https://doi.org/10.1016/j.conbuildmat.2021.123890

Das SK, Dana K (2003) Differences in densification behaviour of K- and Na-feldspar-containing porcelain bodies. Thermochim Acta 406:199–206. https://doi.org/10.1016/S0040-6031(03)00257-0

Diella V, Adamo I, Pagliari L et al (2015) Effects of particle size distribution and starting phase composition in Na-feldspar/kaolinite system at high temperature. J Eur Ceram Soc 35:1327–1335. https://doi.org/10.1016/j.jeurceramsoc.2014.10.035

Drits VA, Derkowski A (2015) Kinetic behavior of partially dehydroxylated kaolinite. Am Mineral 100:883–896. https://doi.org/10.2138/am-2015-5083

Durn G, Ottner F, Slovenec D (1999) Mineralogical and geochemical indicators of the polygenetic nature of terra rossa in Istria, Croatia. Geoderma 91:125–150. https://doi.org/10.1016/S0016-7061(98)00130-X

Ergul S, Sappa G, Magaldi D et al (2011) Microstructural and phase transformations during sintering of a phillipsite rich zeolitic tuff. Ceram Int 37:1843–1850. https://doi.org/10.1016/j.ceramint.2011.03.048

Guatame-García A, Buxton M, Deon F et al (2018) Toward an on-line characterization of kaolin calcination process using short-wave infrared spectroscopy. Miner Process Extr Metall Rev 39:420–431. https://doi.org/10.1080/08827508.2018.1459617

Kalpana M, Tayu A (2020) Light weight steel fibre reinforced concrete: a review. Mater Today Proc 22:884–886. https://doi.org/10.1016/j.matpr.2019.11.095

Kim Y-H, Kim H-Y, Yang K-H, Ha J-S (2021) Effect of concrete unit weight on the mechanical properties of bottom ash aggregate concrete. Constr Build Mater 273:121998. https://doi.org/10.1016/j.conbuildmat.2020.121998

Martínez JD, Betancourt-Parra S, Carvajal-Marín I, Betancur-Vélez M (2018) Ceramic light-weight aggregates production from petrochemical wastes and carbonates ($NaHCO_3$ and $CaCO_3$) as expansion agents. Constr Build Mater 180:124–133. https://doi.org/10.1016/j.conbuildmat.2018.05.281

Milheiro FAC, Freire MN, Silva AGP, Holanda JNF (2005) Densification behaviour of a red firing Brazilian kaolinitic clay. Ceram Int 31:757–763. https://doi.org/10.1016/j.ceramint.2004.08.010

Özkan İ, Yayla Z (2016) Evaluation of correlation between physical properties and ultrasonic pulse velocity of fired clay samples. Ultrasonics 66:4–10. https://doi.org/10.1016/j.ultras.2015.12.008

Real S, Gomes MG, Moret Rodrigues A, Bogas JA (2016) Contribution of structural lightweight aggregate concrete to the reduction of thermal bridging effect in buildings. Constr Build Mater 121:460–470. https://doi.org/10.1016/j.conbuildmat.2016.06.018

Roy A, Singh SK, Banerjee PC et al (2010) Bio-beneficiation of kaolin and feldspar and its effect on fired characteristics of triaxial porcelain. Bull Mater Sci 33:333–338. https://doi.org/10.1007/s12034-010-0051-7

Rutherford G (1987) Results of analyses of two clay samples used by A/S Norsk Leca in the production of insulation materials. Appl Clay Sci 2:193–198. https://doi.org/10.1016/0169-1317(87)90030-5

Sandler A, Meunier A, Velde B (2015) Mineralogical and chemical variability of mountain red/brown Mediterranean soils. Geoderma 239–240:156–167. https://doi.org/10.1016/j.geoderma.2014.10.008

Sattari MT, Apaydın H, Öztürk F (2013) Stochastic operation analysis of irrigation reservoir in low-flow conditions: a case study from Eleviyan reservoir, Iran. Turkish J Agric for 37:613–622. https://doi.org/10.3906/tar-1210-89

Siamardi K (2022) Optimization of fresh and hardened properties of structural light weight self-compacting concrete mix design using response surface methodology. Constr Build Mater 317:125928. https://doi.org/10.1016/j.conbuildmat.2021.125928

Sonuparlak B, Sarikaya M, Aksay IA (1987) Spinel phase formation during the 980 °C exothermic reaction in the kaolinite-to-mullite reaction series. J Am Ceram Soc 70:837–842. https://doi.org/10.1111/j.1151-2916.1987.tb05637.x

Stipičević S, Sekovanić L, Drevenkar V (2014) Ability of natural, acid-activated, and surfactant-modified terra rossa soils to sorb triazine herbicides and their degradation products. Appl Clay Sci 88–89:56–62. https://doi.org/10.1016/j.clay.2013.12.017

Torrent J (2005) Mediterranean soils. In: Encyclopedia of soils in the environment. Elsevier, pp 418–427. https://doi.org/10.1016/B0-12-348530-4/00023-0

Torrent J, Cabedo A (1986) Sources of iron oxides in reddish brown soil profiles from calcarenites in Southern Spain. Geoderma 37:57–66. https://doi.org/10.1016/0016-7061(86)90043-1

Uz V (2010) Using of pyrophyllite bearing red clay for ceramic tile production. Ind Ceram 30:169–175

Vigneron TQG, Vieira CMF, Delaqua GCG et al (2019) Incorporation of mold flux waste in red ceramic. J Mater Res Technol 8:5707–5715. https://doi.org/10.1016/j.jmrt.2019.09.038

Vingiani S, Di Iorio E, Colombo C, Terribile F (2018) Integrated study of red mediterranean soils from Southern Italy. CATENA 168:129–140. https://doi.org/10.1016/j.catena.2018.01.002

Springer Nature or its licensor (e.g. a society or other partner) holds exclusive rights to this article under a publishing agreement with the author(s) or other rightsholder(s); author self-archiving of the accepted manuscript version of this article is solely governed by the terms of such publishing agreement and applicable law.